Volume 1 | Number 1 | Jan 2013 | Pages 1–100

Lab on a Chip

Miniaturisation for chemistry, physics, biology, materials science and bioengineering
www.rsc.org/loc

ROYAL SOCIETY OF CHEMISTRY

ROYAL SOCIETY OF CHEMISTRY

www.rsc.org/loc

A high-power ultrasonic microreactor and its application in gas-liquid mass transfer intensification

Zhengya Dong[a,b], Chaoqun Yao[a,b], Xiaoli Zhang[c], Jie Xu[c], Guangwen Chen[a*], Yuchao Zhao[a], Quan Yuan[a]

[a] *Dalian National Laboratory for Clean Energy, Dalian Institute of Chemical Physics, Chinese Academy of Sciences, Dalian 116023, China, gwchen@dicp.ac.cn*
[b] *University of Chinese Academy of Sciences, Beijing 100049, China*
[c] *Applied Acoustics Institute, Shaanxi Normal University, Xian, Shaanxi 710062, China*

Abstract

Combination of ultrasound and microreactor is an emerging and promising area, but the report of designing high-power ultrasonic microreactor (USMR) is still limited. This work presents a robust, high-power and highly efficient USMR by directly coupling a microreactor plate with a Langevin-type transducer. The USMR is designed as a longitudinal half wavelength resonator, for which the antinode plane of the highest sound intensity is located at the microreactor. According to one dimension design theory, numerical simulation and impedance analysis, a USMR with maximum power of 100 *W* and resonance frequency of 20 kHz was built. The strong and uniform sound field in the USMR was then applied to intensify gas-liquid mass transfer of slug flow in a microfluidic channel. Non-inertial cavitation with multiple surface wave oscillation was excited on the slug bubbles, enhancing the overall mass transfer coefficient by 3.3-5.7 times.

Keywords: Ultrasound; Microchnnel; Microfluidic; Taylor flow; Sonochemistry; Acoustic cavitation

Introduction

Intensification of chemical and biological processes by ultrasound has a long history[1] and has become a popular area named sonochemistry since the early 1980s[2-4]. It was at about the same time that microfluidics emerged[5,6] and since then gained wide applications in biomedical analysis and chemical synthesis[7-9]. Until the beginning of this century ultrasound was gradually applied in microreactors[10-14], which was recently recognized as a very

promising area[15-18]. Due to non-invasive nature[10,19] and strong acoustic effects like radiation force[20] and streaming[21,22], ultrasound can be widely used to manipulate samples[23-27], enhance mixing[28-31]/mass transfer[17,32] and prevent clogging in microreactors[33,34]. On the other hand, with well-defined inner micro-structure, microreactor provides an ideal environment to investigate and control the acoustic cavitation processes[15,35-40], which is the main mechanism for most power ultrasound applications[41-43].

To introduce ultrasound into microfluidic channels, various types of USMR have been reported in literature. In the early stage, microreactors integrated with piezoelectric films were used[11-13,22]. These devices need sophisticated micro-fabrication process and lack generality in operation[15]. Currently, the most common USMR is composed of piezoelectric pieces directly glued to the outer surface of microreactor[19,25] or compressed between the microreactor plates[34]. This kind of USMR is widely used in acoustophoresis[18, 44] and acoustic bubble transducers[23,27,30], since it is easy to fabricate and operate. However, as limited by low tensile strength and heat generation of the piezoelectric ceramic[15], the power load of the piezoelectric piece is usually very low (from milliwatts to a few Watts), which limits its application in area where high power is needed.

In the field of power ultrasound and sonochemistry, Langevin-type ultrasonic transducer (LUT) is often used to generate high-power ultrasound[45-47]. The most convenient way to combine LUT and microreactor is directly immersing the microreactor in a ultrasonic cleaning bath[32,48]. But the water in the bath would also be cavitated, which dissipates a large portion of the input energy[34]. To overcome this issue, Hubner et al.[17] designed a vessel filled with pressured water (*ca* 4.5 bar, the cavitation of the water was suppressed) to transmit the ultrasound from a LUT to the microreactor. This indirect energy input methods has advantages of modularity and temperature control[15,17,49], while the energy transfer efficiency is relatively low, due to the attenuation in the transmission medium and reflection at the liquid/solid interface. Directly coupling LUT with microreactor is the most efficient way to deliver ultrasound into microreactors. For this type of USMR, the key is to design the structure of the LUT and microreactor to ensure a robust, strong and uniform sound field in the microreactor. Tseng et al.[50] recently built a USMR by using a glass plate to connect the LUT and a PDMS microfluidic chip. The acoustic field was coupled into the microfluidic channel via the glass plate's flexural Lamb wave vibration, which is highly sensitive to the thickness and surface structure of the plate. So, the acoustic vibration pattern was altered and vibration amplitude was damped at the region where the PDMS chip is bonded[50]. In this paper, we present a novel high-power USMR with microreactor plate directly coupled with LUT.

The USMR is designed as a longitudinal half wavelength resonator, in which the antinode plane of the highest sound intensity is located at the microreactor plate. Compared to flexural vibration mode, such longitudinal standing wave is more robust, energy efficient[45] and could achieve a quite uniform sound field in the microreactor.

The USMR was then used to intensify the gas-liquid mass transfer in a microfluidic channel. Many research results have shown that mass transfer rate in microreactors is largely imporved compared with conventional equipments[51-54]. As a result, many reactions can be operated in microreactors under much more harsh conditions to increase reaction rate[55]. However, the improvement of mass transfer in microreactors is mainly due to the large specific surface area. The increase of mass transfer coefficient (k_L) is relatively not significant[51-53]. For some reactions of faster kinetics, the mass transfer needs to be further intensified[55,56]. As being able to create turbulence and streaming in the liquid, ultrasound has been used as an effective way in conventional equipments to enhance the gas-liquid mass transfer coefficient[4,57-60]. In this paper, microreactor is combined with ultrasound to intensify gas-liquid mass transfer. Surface wave oscillation and microstreaming was excited on the slug bubbles, enhancing the overall mass transfer coefficient by 3.3-5.7 times.

Building the ultrasonic microreactor
Design of the USMR

LUT is composed of piezoelectric ceramic pieces clamped between the front mass and the back mass, which serve both to protect the piezoelectric ceramic and prevent it from overheating by acting as a heat sink[45,46,61] (see ESI). When operated at resonance frequency, LUT vibrates as a half wavelength resonator[44] at the longitudinal direction, with the antinode plane located at the two ends. As the front mass is usually made of light metal and the back mass heavy metal, the vibration amplitude in the front surface of the transducer is the highest. If we directly couple the microreactor to the front surface of the LUT and let them vibrate as a similar longitudinal half wavelength resonator, the ultrasound would transmit into the microreactor efficiently, where the antinode plane with the highest and uniformly distributed ultrasound intensity is located (Fig. 1a).
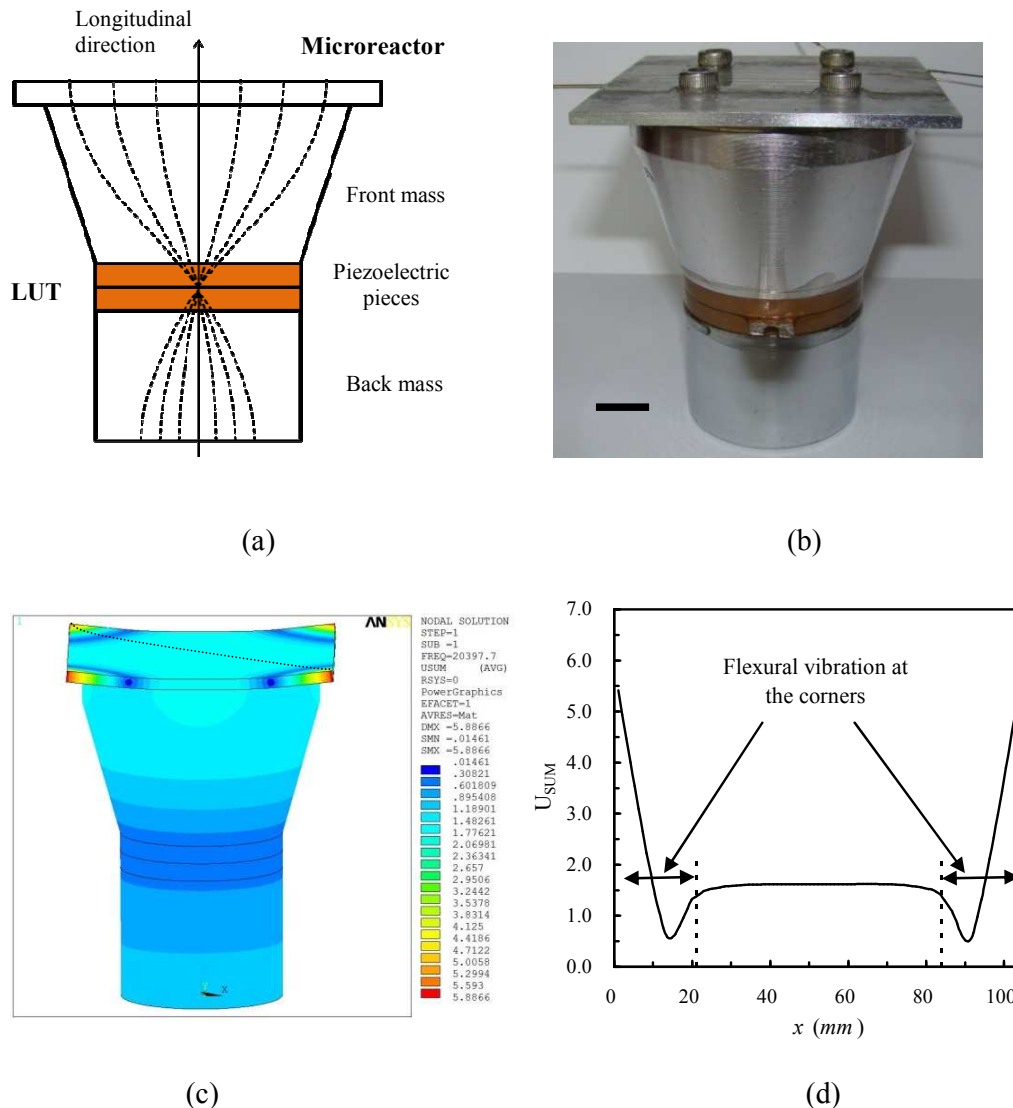
(a)

(b)

(c)

(d)

Fig. 1 (a) Design diagram of the ultrasonic microreactor. The dashed lines represent the half wavelength standing wave (or resonator). (b) Photo of the fabricated ultrasonic microreactor. The scale bar in the figure is 10 *mm*. (c) The simulated vibration displacement distribution of the ultrasonic microreactor at resonance frequency of 20.4 kHz. (d) The simulated vibration displacement distribution (U_{SUM}) along the diagonal line on the surface of the microreactor (as indicated by the dashed line in Fig.1(c)).

To obtain this ideal state, the following aspects have to be emphasized when designing the USMR. 1) The structure of the microreactor needs to match the transducer to ensure pure longitudinal standing wave. The size of the microreactor in the longitudinal direction should be uniform, which means a flat plate is preferred. The size in the transverse direction shouldn't be too much larger than the front surface of the LUT. Otherwise, flexural vibration

4

mode of the microreactor will be excited and coupled with the longitudinal vibration, reducing the efficiency of the resonator[45,61]. 2) The sizes of each part of the USMR should be designed to keep the vibration node located at the piezoelectric pieces, in order to maximize the energy efficiency and lifespan of the piezoelectric element[47]. The node location and the resonance frequency can be predicted by the one dimension design theory[45,61](see ESI), which can be used to guide the size design. 3) The coupling of the microreactor with the front mass should be rigid and without obvious transmission attenuation or reflection. Therefore, the microreactor and the front mass should be made of materials with similar acoustic impedance and coupled with robust method.

Fabrication of the USMR

   Considering our application, we designed and fabricated an USMR with maximum power of 100 *W* and resonance frequency around 20 kHz (Fig. 1b). A commercial LUT (ZFHN-100-21.5, Baoding Zhengjie Electric, China) was purchased (see ESI for more details). The Aluminum alloy (LY12) front mass has a shape of circular truncated cone, which could ensure large radiation area (diameter of the front surface 66 *mm*). A square microreactor plate (made of LY12) with length of 74 *mm* was used. Under the guidance of one dimension design theory, the thickness of the plate was chosen to be 3 *mm*, when the resonance frequency was calculated to be 20.38 kHz and the vibration node located at the upper piezoelectric piece (see ESI for the calculating details). The microreactor plate was then directly attached to the front surface of the LUT by an ultrasonic transmission gel (THD-383, Taiheda, China). To enhance the bonding strength, the two contact surfaces were sandblasted with corundum sand (36 mesh) at first. The connection was further reinforced by four long stainless steel screws (diameter 5 *mm*).

Characterization of the USMR

   The vibration mode of this USMR was then checked by numerical simulation with the ANSYS software. The vibration displacement distribution (Fig. 1c) showed that most part of the USMR is vibrating as a longitudinal half wavelength standing wave at its resonance state. The vibration node of lowest displacement locates in the piezoelectric pieces and the antinode of highest displacement in the microreactor. Only the four corners of the microreactor plate undergo flexural vibration, with the vibration amplitude first dropping near to zero and then rising to a high value near the four vertexes (see Fig.1(d)). This dramatic vibration displacement variation is caused by the uneven excitation at the back of the microreactor, as

the four corners are not covered by the transducer's front surface. Besides these corners, the vibration displacement amplitude in center of the microreactor plate is almost the same, which means a quite uniform sound field (see Fig.1(d)).

The resonance state of the USMR was also characterized by an impedance analyzer (PV70A, Beijing Band Era, China). No obvious flexural vibration peak was observed near the high longitudinal resonance peak in the measured admittance curves (Fig. 2). It indicates that the coupling of flexural vibration with longitudinal vibration is very weak and a pure longitudinal resonator is obtained. When the microreactor was coupled to the transducer, the resonance peak shifted from 21.66 kHz to 20.21 kHz, which was close to the theoretical value above. The measured resonance frequency, dynamic impedance and the quality factor were displayed in Table 1. For a piezoelectric acoustic device, typically the lower is the dynamic impedance, the higher is the quality factor, which means higher electroacoustic transforming efficiency. As showed in Table 1, due to the loading of the microreactor, the dynamic impedance of the USMR increased while the quality factor decreased. During experimental operation, the USMR needed to be sealed by a cover plate and connected to the inlet and outlet tubes, which would further increases the dynamic impedance and decreases the electroacoustic efficiency. To minimize these influences, the microreactor was sealed by a thin transparent polycarbonate film (0.2 *mm* in thickness) with epoxy glue, and connected with small stainless steel capillaries at the inlet and outlet (Fig. 1(b)). Even though those attempts were made, the resonance frequency of the USMR connected to the experiment system still shifted to 20.08 kHz and the quality factor decreased to 503.0 (Table 1).
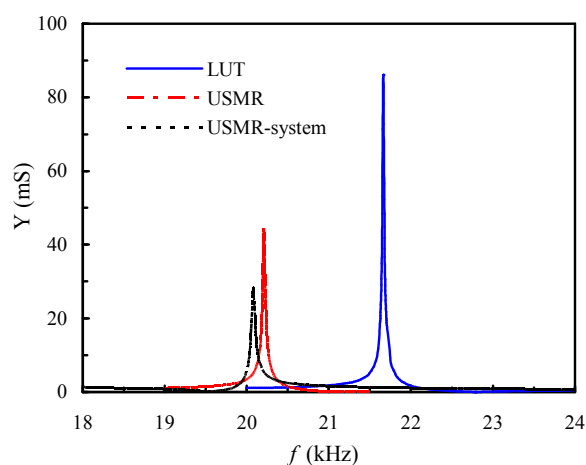

Fig.2 The measured admittance (Y) of the LUT, USMR and USMR connected to system at different frequency.

Table 1 the resonance frequency (f_R), dynamic impedance (R_1) and quality factor (Q_m) measured by the impedance analyzer.

| Parameter	LUT	USMR	USMR-system
f_R (kHz)	21.66	20.21	20.08
R_1 (Ω)	11.67	22.53	35.31
Q_m	1250.3	748.9	503.0

Intensification of the gas-liquid mass transfer
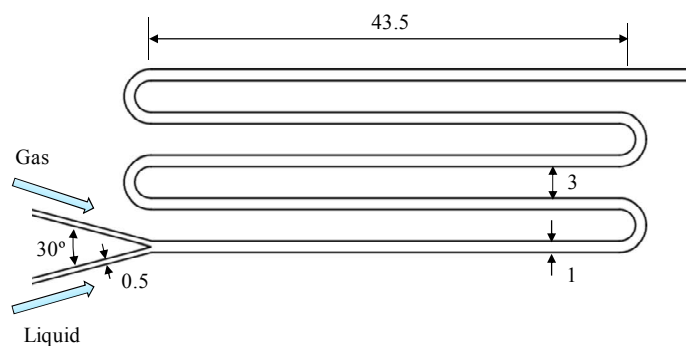
Experimental setup

The efficiency of the USMR was then tested by a gas-liquid mass transfer process. The experimental system consisted of electrical, acoustic, flow and optical subsystems (Fig. 3(a)). In the electrical subsystem, the electrical signal generated by the ultrasonic generator (ZFDY-600FS, Baoding Zhengjie Electric, China) was used to drive the transducer. The effective input power and output wave form were recorded by a power meter and a digital oscilloscope (DS1052E, Rigol, China) respectively. In the acoustic subsystem, the electrical energy was converted into ultrasound wave by the LUT, which was then transmitted into the microchannels (see Fig.3(b)) on the microreactor plate. A sponge bed at the bottom of the transducer was used to support the USMR and isolate the vibration. The ultrasound in the microchannel was then used to intensify the gas-liquid two phase flow, which was supplied by the flow subsystem. Physical absorption of pure CO_2 into deionized water was used. The mass transfer process was monitored by the optical subsystem. It consisted of a light source, two optical fiber for concentrated illumination, a macro lens and a high speed camera (Phantom M310, Vision Research, USA). Other details about the experimental setup can be found in ESI.

Before the mass transfer experiment, the actual working frequency of the system was first determined by sweeping the driving frequency of ultrasonic generator around the designed resonance frequency. The frequency corresponding to the maximum input power was chosen as the working frequency. The value determined by this method was 19.70 kHz, which was then fixed in the following experiment. To alleviate the thermal effect of ultrasound, an air fan with power of 20 *W* was put against the USMR to cool the system. Besides, to avoid significant temperature rise, the ultrasonic generator was only turned on for a few minutes for each operating condition, during which the video of the gas-liquid two phase flow was recorded and then used for mass transfer measurement. When one experiment was completed, the ultrasonic generator was then turned off, while the air fan still on to cool the system. Next

experiment was conducted only when the temperature of the system was reduced to room temperature. The temperature rise at each operating condition was kept under 3 $^{\circ}$C. The effect of this small temperature rise on the mass transfer measurement can be neglected at the present experiments, as was discussed in detail in ESI.
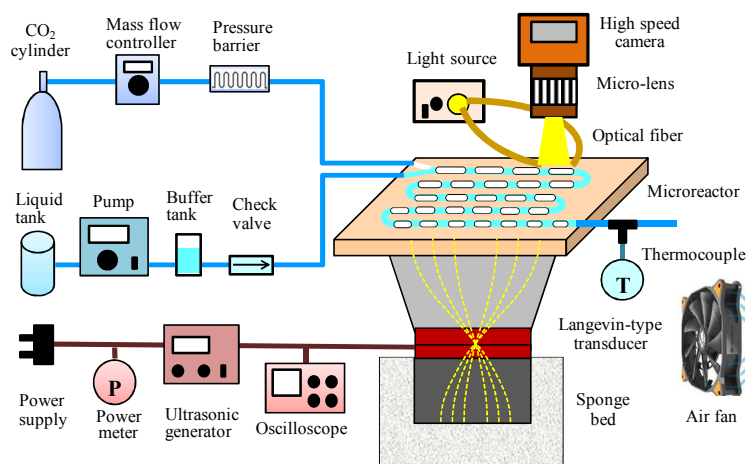
(a)

(b)

Fig. 3(a) Schematic of the experimental setup. (b) The structure of the microchannel in the microreactor. The width of the inlet channels is 500 μm. The width of the main channel is 1 mm. The depth of all the channels is 1 mm.

Slug bubble oscillation in USMR

Before turning on the ultrasonic generator, a stable gas-liquid slug flow (or Taylor flow)[62,63] was formed in the microfluidic channel. Due to the absorption of CO_2, the size of the gas bubbles decreased while moving downstream in the channel. When the ultrasound was exerted, the flowing slug bubbles oscillated vigorously (see ESI). The detail of the bubble oscillation was recorded by the high speed camera at frame rate of 100 000 fps (see video1 in

ESI). Since the electrical signal supplied to the LUT changed periodically (see ESI), the oscillation of the gas bubbles also had a periodical behavior.

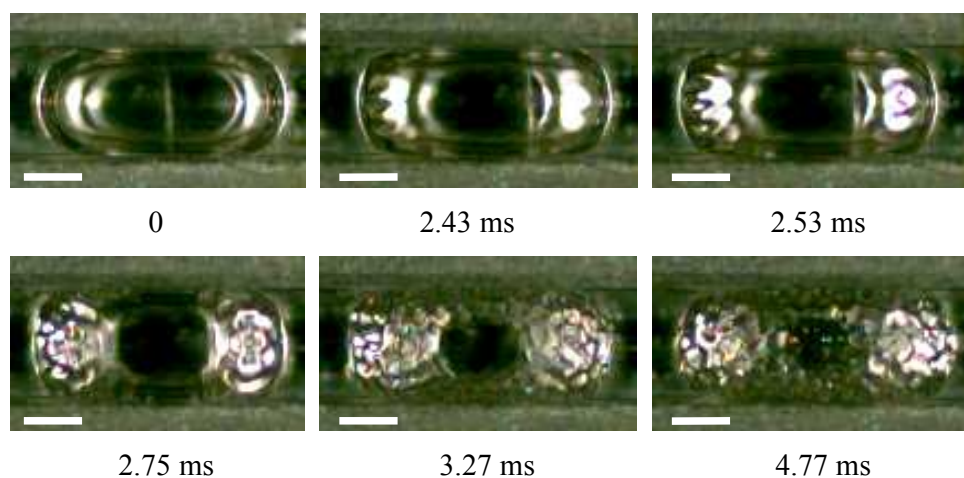|		
0	2.43 ms	2.53 ms
2.75 ms	3.27 ms	4.77 ms

Fig. 4 Bubble oscillation at increasing ultrasound intensity from left to right. The six pictures were captured from video1 at different time, as indicated by the tags. As the input voltage increases with time at this period, the ultrasound intensity also increases with the time. The scale bar in all the figures is 500 μm.

As shown in Fig. 4 and video1, the slug bubble's surface vibrated fiercely without collapse, indicating that it undergoes non-inertial cavitation. Compared to the wild inertial cavitation, bubble oscillation in non-inertial cavitation is more stable. It includes various oscillation modes depending on the acoustic pressure[41,42,64]. When the applied acoustic pressure is low, the bubble undergoes breathing oscillation mode with pulsation of the bubble volume. When the acoustic pressure exceeds a threshold, shape oscillation with many surface wave modes is excited. The surface wave mode with the lowest threshold is the Faraday wave mode, which appears as symmetrical peaks and valleys on the bubble surface. At higher acoustic pressure, many surface wave modes are superimposed, which leads to chaotic motion of the bubble surface[15,65,66]. The bubble in our experiment was confined by the microchannel and had a slug shape, but the cavitation behavior still corresponded to the above fact. As shown in video S1 and Fig. 3, with the increasing of the input electrical voltage, the bubble oscillation changed from volume pulsation to regular surface wave oscillation, and finally to chaotic surface distortion. Meanwhile, the area of significant surface distortion is increased. It started from the free bubble tips, and then gradually invaded the bubble waist confined by the microfluidic channel wall, and finally expanded to the entire bubble surface. It indicated that for confined

bubble surface, higher acoustic intensity was required to excite the surface wave modes than the free bubble surface.

Gas-liquid mass transfer intensification results

Due to the mass transfer of CO_2 from gas into water, the length of the slug bubbles decreases while moving downstream the channel. The faster is the mass transfer process, the higher is the decreasing rate of the bubble length. We have developed a unit cell model to analysis this mass transfer process[67,68]. An exponential type equation was obtained to describe the relationship between the bubble length and its location

$$L_B = m_1 + m_2 e^{-\frac{k_L a}{j_L}x} \tag{1}$$

where j_L is the superficial velocity of liquid. Parameter m_1 and m_2 depend only on the experiment condition and the channel size. So, the overall volumetric mass transfer coefficient $k_L a$ can be determined by curve fitting the bubble length at different locations.
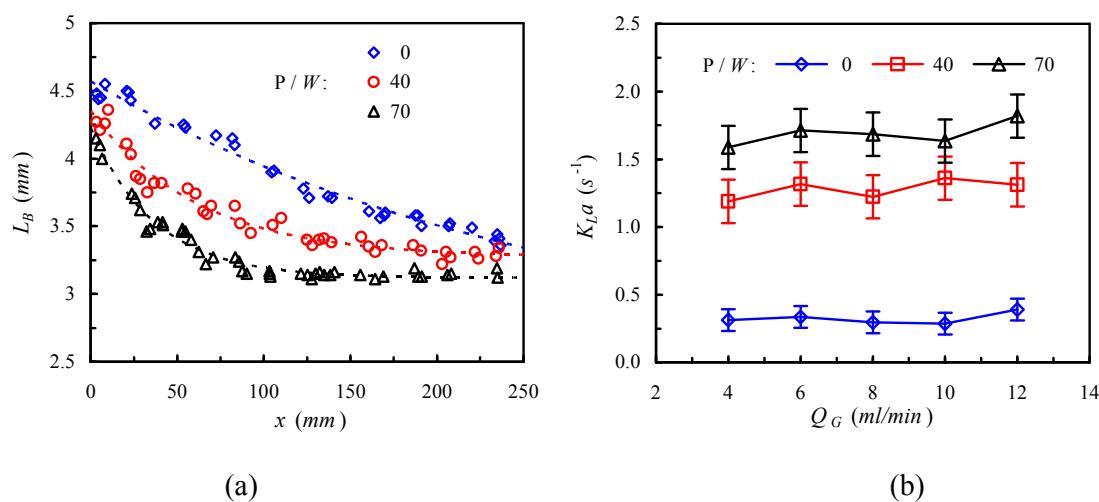

(a)   (b)

Fig. 5 (a) The length of a CO_2 slug bubble at different locations in the channel under different ultrasound power (Q_L=4 *ml/min*, Q_G=8 *ml/min*). The dashed lines are fitting curves according to Eq. (1). (b) Mass transfer coefficient of the gas-liquid flow at different gas flow rate with ultrasound power 0 *W*, 40 *W* and 70 *W* (Q_L=4 *ml/min*). Each point was measured at least for two times. For each power level, the maximum deviation was chosen for all points.

The bubble lengths at different locations in the channel were recorded and measured by a high speed camera. As shown in Fig. 5(a), without ultrasound irradiation, the bubble length decreases at a very slow rate. When ultrasound is introduced, the bubble length decreases

faster and quickly approaches the equilibrium length when the water is almost saturated. Higher ultrasound intensity leads to larger decrease rate of bubble length. The overall volumetric mass transfer coefficients were calculated by fitting the experiment data with Eq. (1). As shown in Fig. 5(b), when ultrasound is not introduced, the overall volumetric mass transfer coefficient ranges from 0.29 to 0.39 s^{-1}, which is in consistent with results in literature[69,70,71] for similar channel size and flow rates. With increasing in gas flow rate, the mass transfer coefficient increases slightly, since larger bubble length is not beneficial for mass transfer. This phenomena have also been observed before[51,67,72]. Fig. 5(b) also shows that mass transfer can be greatly enhanced when ultrasound is present and mass transfer coefficient increases with increase of ultrasound power. In our experiments, the mass transfer coefficient ranges from 1.2 to 1.8 s^{-1}, which is about 3.3-5.7 times larger than the conditions without ultrasound. This significant mass transfer coefficient improvement is mainly caused by the fierce bubble oscillation phenomenon described in the last section. Surface wave oscillation of the slug bubble can dramatically increase the gas-liquid contact area. Besides, the fierce bubble oscillation could also create turbulence and streaming in the liquid near the interface, which further enhance the mass transfer coefficient. In fact, as a steady flow formed by the viscous dissipation of acoustic energy in the boundary layer of an oscillating bubble, cavitaion microstreaming is always accompanied with surface wave oscillation [15,21,31,41,73]. It has been widely used to pump fluid[30,74] and enhance mixing[19,21,27,29,31,40]. It can be expected that this kind of microstreaming is also present near the oscillating slug bubbles in our experiment, which would significantly accelerate the gas-liquid mass transfer process.

This enhancement of mass transfer coefficient in our USMR is much higher than that in conventional ultrasonic reactors, which is usually between 10% and 110%[4,57,59,60]. There are two possible reasons. Firstly, the ultrasound power density in our USMR (0.13-1.4 *W/ml*, see ESI for more details) is higher than that in conventional reactors (usually between 0.05-0.6 *W/ml*), due to the relatively small volume of the microreactor and high energy efficiency of the USMR design. Secondly, the intensification mechanism in our USMR—non-inertial cavitation with fierce surface wave oscillation and microstreaming is more stable and uniformly distributed than in conventional reactors. As the sound field in the microreactor plate is quite uniform, all the bubbles in the microreactor are in fierce oscillation (see Fig. S3(b) in ESI), which is difficult to achieve in conventional large ultrasonic reactors[4,16,58,59].

Conclusion

A robust USMR vibrating as a half wavelength resonator was designed and fabricated,

according to one dimension design theory, numerically simulation and impedance analysis. A strong and uniform sound field is generated in the microreactor. As the USMR is built by directly coupling a microreactor plate to a commercial available LUT (~US$15), the fabrication process is relatively simple and low cost. The design concept and method can be used to fabricate USMR with higher power, larger volume and higher throughput. The gas-liquid mass transfer was significantly enhanced in our USMR, due to the high ultrasound power density, stable and uniformly distributed intensification mechanism—fierce surface wave oscillation of the slug bubble. If the electronic subsystem (especially the wave form of the ultrasonic generator) is further optimized, the mass transfer enhancement would be larger. This USMR can be an efficient and versatile tool for the microfluidic communities, which could be applied to intensify mixing and chemical reactions, prevent clogging, handle biomaterials, study acoustic cavitation processes and so on.

References

1   R.W. Wood and A. L. Loomis, *Philos. Mag.*, 1927, **4**, 414-436.

2   K. S. Suslick, *Ultrasound: its chemical, physical, and biological effects,* VCH Publishers, 1988

3   A. Stankiewicz, *Chem. Eng. Res. Des.*, 2006, **84**, 511-521

4   P. R. Gogate, V. S. Sutkar and A. B. Pandit, *Chem. Eng. J.*, 2011, **166**, 1066-1082

5   S. C. Terry, J. H. Jerman and J. B. Angell, *IEEE Trans. Electron Devices*, 1979, **26**, 1880-1886

6   D. B. Tuckerman and R. F. W. Pease, *IEEE Electron Device Lett.*, 1981, **2**, 126-129

7   K. Jahnisch, V. Hessel, H. Löwe and M. Baerns, *Angew. Chem. Int. Ed.*, 2004, **43**, 406-446.

8   G. M. Whitesides, *Nature*, 2006, **442**, 368-373.

9   R. L. Hartman and K. F. Jensen, *Lab Chip*, 2009, **9**, 2495-2507.

10   K. Yasuda, *Sens. Actuators B*, 2000, **64**, 128-135

11   Z. Yang, S. Matsumoto, H. Goto, M. Matsumoto and R. Maeda, *Sens. Actuators A*, 2001, **93**, 266-272

12   J. C. Rife, J. S. Horwitz, M. I. Bell, M. N. Kabler, R. C. Y. Auyeung and W. J. Kim, S*ens. Actuators A*, 2000, **86**, 135-140

13   G. G. Yaralioglu, I. O. Wygant, T. C. Marentis and B. T. Khuri-Yakub, *Anal. Chem.*, 2004, **76**, 3694-3698

14   M. Bengtsson and T. Laurell, *Anal. Bioanal. Chem.*, 2004, **378**, 1716-1721

15   Y. Iida, T. Tuziuti, K. Yasui, A. Towata and T. Kozuka, *Ultrason. Sonochem.*, 2007, **14**, 621-626

16   D. F. Rivas, P. C. Cintas and Han J. G. E. Gardeniers, *Chem. Commun.*, 2012, **48**, 10935-10947

17   S. Hubner, S. Kressirer, D. Kralisch, C. Bludszuweit-Philipp, K. Lukow, I. Janich, A. Schilling, H. Hieronymus, C. Liebner and K. Jahnisch, *ChemSusChem*, 2012, **5**, 279-288

18   H. Bruus, J. Dual, J. Hawkes, M. Hill, T. Laurell, J. Nilsson, S. Radel, S. Sadhal and M. Wiklund, *Lab Chip*, 2011, **11**, 3579-3580

19   D. Ahmed, X. Mao, B. K. Juluri and T. J. Huang, *Microfluid Nanofluid*, 2009, **7**, 727-731

20   L. A. Kuznetsova and W. T. Coakley, *Biosens. Bioelectron.*, 2007, **22**, 1567-1577

21   M. Wiklund, R. Green and M. Ohlin, *Lab Chip*, 2012, **12**, 2438-2451

22   L. Johansson, S. Johansson, F. Nikolajeff and S. Thorslun, *Lab Chip*, 2009, **9**, 297-304

23   M. V. Patel, A. R. Tovar and A. P. Lee, *Lab Chip*, 2012, **12**, 139-145

24   P. Marmottant and S. Hilgenfeldt, *Proc. Natl. Acad. Sci. USA*, 2004, **101**, 9523-9527

25   C. Wang, S. V. Jalikop and S. Hilgenfeldt, *Biomicrofluidics*, 2012, **6**, 012801

26   D. Rabaud, P. Thibault, M. Mathieu and P. Marmottant, *Phys. Rev. Lett.*, 2011, **106**, 134501

27   A. Hashmi, G. Yu, M. Reilly-Collette, G. Heiman and J. Xu, *Lab Chip*, 2012, **12**, 4216-4227

28   R. H. Liu, J. Yang, M. Z. Pindera, M. Athavale and P. Grodzinski, *Lab Chip*, 2002, **2**, 151-157

29 D. Ahmed, X. Mao, J. Shi, B. K. Juluri and T. J. Huang, *Lab Chip*, 2009, **9**, 2738-2741

30 A. R. Tovar and A. P. Lee, *Lab Chip*, 2009, **9**, 41-43

31 C. Wang, B. Rallabandi and S.Hilgenfeldt, *Phys. Fluids*, 2013, **25**, 022002

32 S. Aljbour, T. Tagawa and H. Yamada, *Ind. Eng. Chem.*, 2009, **15**, 829-834

33 R. L. Hartman, J. R. Naber, N. Zaborenko, S. L. Buchwald and K. F. Jensen, *Org. Process Res. Dev.*, 2010, **14**, 1347-1357

34 S. Kuhn, T. Noel, L. Gu, P. L. Heider and K. F. Jensen, *Lab Chip*, 2011, **11**, 2488-2492

35 A. Stankiewicz, *Ind. Eng. Chem. Res.*, 2007, **46**, 4232-4235

36 Y. Iida, K. Yasui, T. Tuziuti, M. Sivakumar and Y. Endo, *Chem. Commun.*, 2004, **20**, 2280-2281

37 D. F. Rivas, M. Ashokkumar, T. Leong, K. Yasui, T. Tuziuti, S. Kentish, D. Lohse and H. J. G. E. Gardeniers, *Ultrason. Sonochem.*, 2012, **19**, 1252-1259

38 T. Tandiono, S. W. Ohl, D. S. W. Ow, E. Klaseboer, V. V. Wong, R. Dumkec and C. D. Ohl, *Proc. Natl. Acad. Sci. USA*, 2011, **108**, 5996-5998.

39 T. Tandiono, S. W. Ohl, D. S. W. Ow, E. Klaseboer, V. V. Wong, A. Camattari and C. D. Ohl, *Lab Chip*, 2010, **10**, 1848-1855

40 A. Ozcelik, D. Ahmed, Y. Xie, N. Nama, Z. Qu, A. A. Nawaz and T. J. Huang, *Anal. Chem.* 2014, **86**, 5083-5088

41 T. G. Leighton, *The Acoustic Bubble*, Academic Press Limited, London, 1994.

42 T. G. Leighton, *Prog. Biophys. Mol. Biol.*, 2007, **93**, 3-83

43 J. Rooze, E.V. Rebrov, J. C. Schouten and J.T.F. Keurentjes, *Ultrason. Sonochem.*, 2013, **20**, 1-11

44 A. Lenshof, M. Evander, T. Laurell and J. Nilsson, *Lab Chip*, 2012, **12**, 684-695

45 S. Lin, *The mechanism and design of ultrasound transducer*, Science Press, Beijing, 2004 (in Chinese)

46 T. J. Mason and D. Peters, *Applied Sonochemistry: Uses of Power Ultrasound in Chemistry and Processing*, Wiley-VCH, 2002

47 A. Mathieson, A. Cardoni, N. Cerisola, and M. Lucas, *IEEE Trans. Sonics Ultrason.*, 2013, **60**, 1126-1133

48 T. Horie, M. Sumino, T. Tanaka, Y. Matsushita, T. Ichimura and J. Yoshida, *Org. Process Res. Dev.*, 2010, **14**, 405-410

49 *WO Pat.*, 2011 023761 A1, 2011

50 Q. Tseng, A. M. Lomonosov, E. E. M. Furlong and C. A. Merten, *Lab Chip*, 2012, **12**, 4677-4682

51 J. Yue, G. W. Chen, Q. Yuan, L. Luo and Y. Gonthier, *Chem. Eng. Sci.*, 2007, **62**, 2096-2108

52 P. Sobieszuk, J. Aubin and R. Pohorecki, *Chem. Eng. Technol.* 2012, **35**, 1346-1358

53 M. J. Nieves-Remacha, A. A. Kulkarni and K. F. Jensen, *Ind. Eng. Chem. Res.*, 2013, **52**, 8996−9010

54 M. N. Kashid, A. Renken and L. Kiwi-Minsker, *Chem. Eng. Sci.,* 2011, **66**, 3876-3897

55 V. Hessel, D. Kralisch, N. Kockmann, T. Noel and Q. Wang, *ChemSusChem*, 2013, **6**, 746-789

56 N. Kockmann, *Transport phenomena in micro process engineering: Fundamentals, devices, fabrication, and applications*, Springer, Berlin, 2008

57 M. L. Cadwell and H. S. Fogler, *Chem. Eng. Prog. Symp. Series,* 1971, **67**, 124-127

58 N. S. Herran, J. L. Casas Lopez and J. A. S. Pere, *Ind. Eng. Chem. Res.*, 2012, **51**, 2769-2774

59 A. Kumar, P. R. Gogate, A. B. Pandit, H. Delmas and A. M. Wilhelm, *Ind. Eng. Chem. Res.*, 2004, **43**, 1812-1819

60 N. Gondrexon, V. Renaudin, P. Boldo, Y. Gonthier, A. Bernis and C. Petrier, *Chem. Eng. J.*, 1997, **66**, 16-21.

61 M. D. McCollum, B. F. Hamonic and O. B. Wilson, *Transducers for Sonics and Ultrasonics*, Technomic, Lancaster, PA, 1993

62 Y. C. Zhao, G. W. Chen, C. B. Ye and Q. Yuan, *Chem. Eng. Sci.*, 2013, **87**, 122-132

63 C. Q. Yao, Y. C. Zhao, C. B. Ye, M. H. Dang, Z. Y. Dong and G. W. Chen, *Chem. Eng. Sci.*, 2013, **95**, 246-256

64 P. R. Birkin, D. G. Offin, C. J. Vian, T. G. Leighton and A. O. Maksimov, J. *Acoust. Soc. Am.*, 2011, **130**, 3297-3308

65 D. G. Offin, P. R. Birkin and T. G. Leighton, *Electrochem. Commun.*, 2007, **9**, 1062-1068

66 P. R. Birkin, Y. E. Watson and T. G. Leighton, *Chem. Commun.*, 2001, **24,** 2650-2651

67 C. Q. Yao, Z. Y. Dong, Y. C. Zhao and G. W. Chen, *Chem. Eng. Sci.*, 2014, **112**,

15-24

68 C. Q. Yao, Z. Y. Dong, Y. C. Zhao and G. W. Chen, *Chem. Eng. Sci.*, 2015, **123**, 137-145

69 C. O. Vandu, H. Liu and R. Krishna, *Chem. Eng. Sci.*, 2005, **60**, 6430-6437

70 J. M. van Baten and R. Krishna, *Chem. Eng. Sci.*, 2004, **59**, 2535-2545

71 J. Yue, L. Luo, Y. Gonthier, G. W. Chen and Q. Yuan, *Chem. Eng. Sci.*, 2009, **64**, 3697-3708

72 J. Tan, Y. C. Lu, J. H. Xu and G. S. Luo, *Chem. Eng. J.*, 2012, **181**, 229-235.

73 S. A. Elder, *J. Acoust. Soc. Am.*, 1959, **31**, 54-64.

74 K. Ryu, S. K. Chung and S. K. Cho, *J. Lab. Autom.*, 2010, **15**, 163-171